Proceedings of the 25th International Conference on
Port and Ocean Engineering under Arctic Conditions
June 9-13, 2019, Delft, The Netherlands

Use of satellite remote sensing to study wave-ice interactions in the marginal ice zone – A review

Dennis Monteban[1,2], Raed Lubbad[2], Jens Olaf Pepke Pedersen[1]
[1] Technical University of Denmark (DTU), Space department, Lyngby, Denmark
[2] The Norwegian University of Science and Technology (NTNU), Trondheim, Norway

Abstract

Predicting the wave climate in the Polar regions is vital for navigation and offshore operation safety. These predictions are nowadays made using numerical models based on different theories for wave-ice interactions. To date, hardly any field measurements exist that can be used to validate the proposed theoretical models. Remote sensing observations, on the other hand, have a great potential and they are gaining a widespread interest due to the large amounts of data that can be collected continuously over an extensive area.

In this study, we discuss the use of satellite remote sensing to improve our understanding of wave-ice interactions. Three different types of satellite remote sensing are reviewed, including optical, altimetry and synthetic aperture radar (SAR). We present examples of such data over the Barents Sea, where new in situ data are available. These in situ data, which were collected during the *Barents Sea Metocean and Ice Network* (BaSMIN) field campaign, are used to illuminate the review.

Optical data provide high quality and high-resolution images. However, just a small portion of such data are useful to study wave-ice interactions because only images acquired with daylight and cloud free conditions can be processed. Imagery over our study site reveal a tremendous amount of detail of the sea ice, including a diffusive and compact ice edge. Altimetry data provide accurate wave height information up to the ice edge. Wave height data are collected over our study site and validated with buoy measurements. Since the Polar regions are often dark and cloud covered, active microwave sensors such as SAR are the most valuable source of information in these regions. Four different applications of SAR are reviewed: imaging of ocean waves within the ice cover and determination of the ice edge, ice type and floe size distribution. Regarding ocean waves in sea ice, SAR can provide information on wave attenuation, the change in peak wavelength and the shift in dominant wave direction.

KEY WORDS: Marginal ice zone; Sea ice; Remote sensing; Sentinel missions; BaSMIN measurement programme

1. Introduction

Consequences of a warmer climate and warmer sea temperatures are thawing of permafrost, decreasing sea ice extent and increasing ice sheet melt causing changes in relative sea level. The longer open water seasons and increasing storminess will result in an increased rate of coastal erosion in the Arctic (Solomon, 2005). This increasing rate of coastal erosion is further enhanced by thawing of permafrost leaving many coastal communities and facilities exposed to higher risks. Due to a reduced sea ice cover it is also very likely that commercial activities in the Arctic such as marine transport and access to and recovery of resources (e.g., oil) increases (ACIA, 2004).

For safe marine transport in the Arctic and safe offshore operations, accurate predictions of the wave climate are of utmost importance. Hindcasts and forecasts of the wave climate are nowadays often made using numerical wave models. These models have had a long development history (Komen et al., 1994), but with a focus on mid-latitudes. Due to retreat of the sea ice cover, the economic interest in the Arctic has increased and hence, a numerical wave model that can be applied in ice-covered oceans is vital. To be able to apply wave models in the Arctic, the interaction between sea ice and ocean waves needs to be considered. Including wave-ice interactions is not straightforward as it is a strongly coupled problem: the ice affects the waves by refraction, reflection, attenuation, scattering and changes the dispersion relation (e.g., Squire et al. 1995; Squire 2007). On the other hand, the waves also alter the sea ice cover, for instance by ice breakup (e.g., Kohout et al., 2016).

A major obstacle for the development of ice modules in operational numerical wave models, is the need of validation data (Broström and Christensen, 2008). Data of ocean waves propagating into the marginal ice zone (MIZ) can be collected during measurement campaigns, acquired by remote sensing or simulated in the laboratory. Laboratory experiments have the advantage that many environmental parameters can be controlled and therefore isolate the variables of interest. However, only high frequency waves can be generated, and the scaling effects make the generalization of the results extremely difficult (Collins et al., 2017). In situ data collected in the field does not have scaling issues due to its natural setting and typically provides time series, i.e., the temporal domain. However, the acquired data are sparse and have proved to be challenging and costly to collect in the harsh environment of the Polar regions. Remote sensing, on the other hand, provides continuous data acquired over a large area, i.e., in the spatial domain. Moreover, the cost of collecting these data is limited compared to in situ measurements.

This study focusses on the use of satellite remote sensing observations to study the interaction between ocean waves and sea ice. A review is presented and in addition, we use remote sensing data that were acquired over the Barents Sea. New in situ data is available here that was collected during the *Barents Sea Metocean and Ice network* (BaSMIN) measurement campaign, which will be introduced in Section 2. The additional remote sensing data is used to illuminate the review and by combining with in-situ data, a better picture of the study site is obtained. Moreover, the remote sensing observations can be verified and validated with the in-situ measurements. All the satellite data presented here are acquired by the Sentinel missions from the European Space Agency (ESA), which can freely be downloaded from ESA's Sentinel Data Hub. Three different satellite remote sensing techniques are presented herein including optical, altimetry and synthetic aperture radar (SAR) techniques. Optical imagery obtained by the Sentinel-2 constellation is presented in Section 3. Sentinel-3 altimetry data are presented in Section 4 and validated with buoy measurements. SAR is introduced in Section 5 and four of its applications are presented, including imaging of ocean waves (in the open ocean and within the sea ice) and the determination of the ice edge, ice type and floe size distribution. In addition, some Sentinel-1 SAR data are presented as an example. Finally, a conclusion is given in Section 6.

2. BaSMIN measurement programme

The BaSMIN field campaign took place from October 2015 until October 2018 and was executed by Fugro GEOS Ltd on behalf of Equinor (former Statoil). The bathymetry of the Barents Sea and the measurement locations are presented in Figure 1. In total, there were five wavescan moorings, one seabed mooring and five ice profiling moorings. The wavescan moorings measured the seawater and atmospheric temperature, salinity, atmospheric pressure and humidity, and wave parameters. At the ice mooring locations, the ice and current velocity, ice draft, seawater temperature, salinity and pressure were measured. For this project, we used the significant wave height from the buoys to compare with the values derived from altimetry. The measured ice draft at the ice mooring stations is used to see whether ice is present, which is compared with the sea ice edge determination from SAR data.

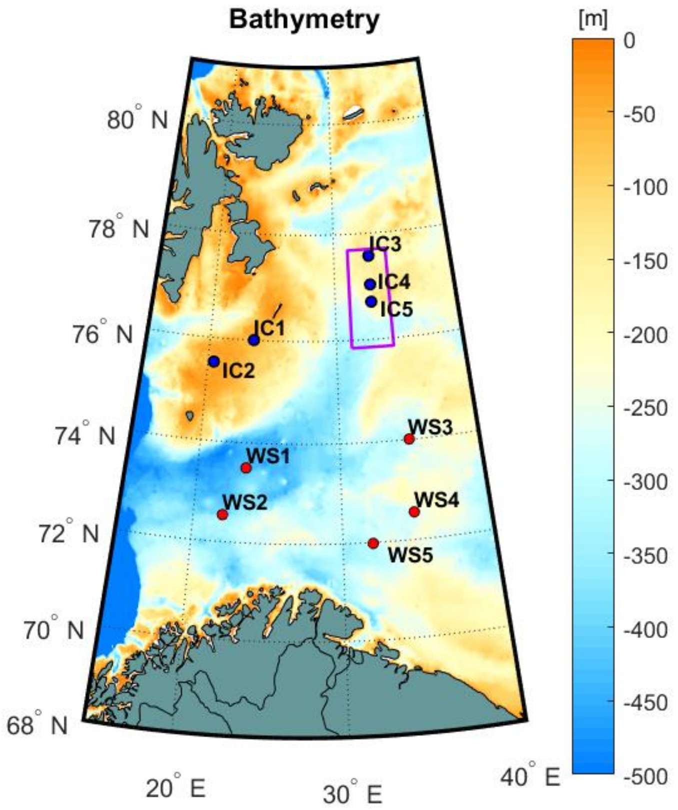

Figure 1. Bathymetry map of the Barents Sea, where the BaSMIN measurement programme took place. The wavescan (WS) moorings are indicated with the red dots and the ice profiling moorings (IC) are shown with the blue dots. The purple rectangle is the extent of the Sentinel-2 imagery, presented in Figure 2. The bathymetry data is taken from the International Bathymetric Chart of the Arctic Ocean (Jakobsson et al., 2012).

3. Optical (Sentinel-2)

The Sentinel-2 constellation consists of twin satellites that follow the same orbit and are phased at 180°. The satellites carry a Multispectral Instrument (MSI) and have the objective of providing high-resolution images at a high revisit frequency (Drusch et al., 2012). The revisit frequency of the twin satellites combined is 5 days. Furthermore, the Sentinel-2 has 13 different spectral bands at a resolution of 10, 20 and 60 meters, depending on the spectral band. A major limitation of the multispectral instrument is that it requires daylight and cloud-free conditions. This severely limits the amount of good and useful images and caused the development of optical techniques to be quite limited (Kudryavtsev et al., 2017).

The high-resolution optical images from Sentinel-2 can be used to observe the ice from above, as illustrated in Figure 2 for our study site. The figure shows Sentinel-2 images of the ice edge close to ice moorings IC3, IC4 and IC5 (see Figure 1), with a resolution of 10 meter. The ice edge is shown on the 2nd of April 2017 in Figure 2a and on the 9th of April 2017 in Figure 2b. The image acquired on the 2nd of April is a good example of a diffuse ice edge, which is characterised by a poorly defined ice edge, an area of dispersed ice and is usually observed at the leeward side. The wind was blowing roughly from north-west for more than 4 days straight before the satellite passed, causing the area of ice to be on the leeward side. Figure 2b shows an example of a compact ice edge. There is a clearly defined ice edge that is compacted by the wind. The wind came from the southeast for approximately 2 days before the image was acquired and therefore the ice edge is on the windward side. Furthermore, Figure 2 provides

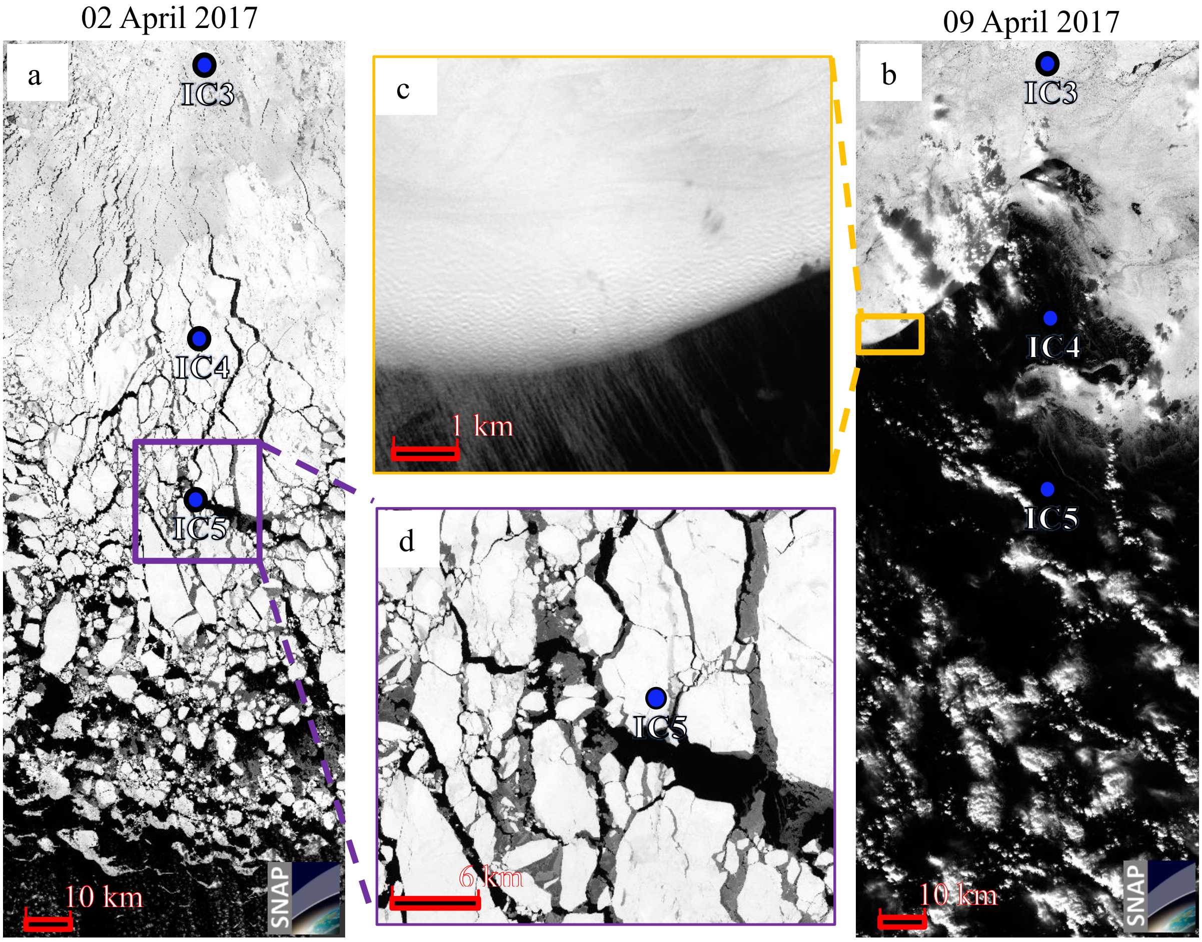

Figure 2. Sentinel-2 imagery (spectral band B4) of the ice edge on the 2nd of April 2017 (panel a) and the 9th of April 2017 (panel b). The extent of panel a and b is indicated in Figure 1. Panel c shows a magnification of the ice edge on the 9th of April. Panel d is a magnification around ice mooring IC5 on the 2nd of April 2017.

magnified images at two locations where a significant amount of detail can be observed. In Figure 2c, waves are visible within the ice at the ice edge. Figure 2d shows the area around ice mooring IC5 and here we can see an example of ice break-up, resulting in ice floes of different sizes, with newly formed ice in between.

Beside the qualitative analysis of the images to observe and understand the ice conditions, a method was developed by Kudryavtsev et al. (2017) to quantitatively retrieve two-dimensional ocean wave spectra from sun glitter imagery. This method uses reflected sunlight (brightness) from the water surface, converted into sea surface elevations in order to perform spectral analysis. However, the method requires a good alignment of the sun, the ocean surface and the satellite. This condition is only met at mid latitudes and not at the high latitude of the Barents Sea.

4. Altimetry (Sentinel-3)

The Sentinel-3 constellation also consists of twin satellites. Sentinel-3 has the objective to deliver operational land and ocean observations. Some of the products that are provided are: sea surface height, ocean surface wind speed, sea surface temperature, significant wave height and land ice/snow surface temperature (European Space Agency, 2013). The satellite carries four main instruments: Ocean and Land Colour Instrument (OLCI), Sea and Land Surface Temperature Instrument (SLSTR), SAR Radar Altimeter (SRAL) and Microwave Radiometer (MWR).

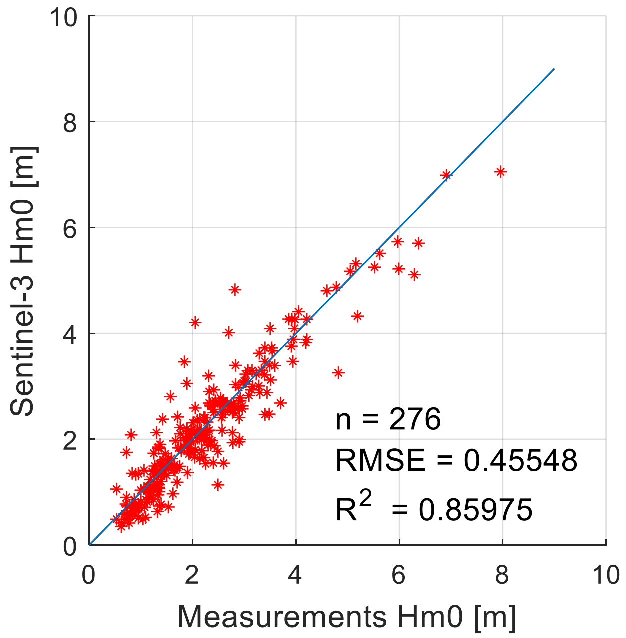

Figure 3. Comparison of the derived significant wave height (Hm0) by the Sentinel-3 constellation and the buoy measurements. Data is included for the period 01-01-2018 until 01-10-2018 from the five wavescan moorings (WS 1-5). Satellite altimetry tracks that pass the wave buoys within 20 km are used, which resulted in 276 observations.

The significant wave height is provided along the track of the satellite from the SRAL instrument. The inter-track distance is 54 km for the two satellites combined. Further, the nadir resolution of the SRAL is more than 2 km and the revisit time is 27 days. The SRAL instrument on the Sentinel-3 satellite can measure significant wave heights within the range of 0.5-20 m, with an error of approximately 4%. (European Space Agency, 2012). In Figure 3 the observations of the Sentinel-3 are plotted against the measurements at the wavescan moorings WS1 to WS5 for the year 2018. Tracks are considered if they pass a wave buoy within 20 km. A total of 276 tracks met this criterion and the observations of the Sentinel-3 are in good agreement with the measurements. A root mean square error (RMSE) of 0.46 and an R-squared value fit to the x=y regression line is 0.86. The information from satellite altimetry has proven to be very accurate (e.g., Vu et al. 2018) and provides additional wave height data over a larger spatial scale than provided by the wave buoys, although the data are still quite sparse. More altimetry satellites are available (e.g., Envisat, SARAL, CryoSat) whose data can be utilised.

In addition to providing information on the ocean waves, altimetry has also been used to estimate sea ice thickness (e.g., Guerreiro et al., 2017; Tilling et al., 2018) and detect open water areas in sea-ice regions (Müller et al., 2017). The estimation of the ice thickness is based on observations of the sea-ice freeboard. The main uncertainty involved when using the freeboard is the presence of snow as it influences the freeboard to a great extent.

5. Synthetic aperture radar (Sentinel-1)

The first SAR satellite was Seasat, which was launched in 1978 (Born et al., 1979). Since then, SAR satellites have provided a tremendous amount of data to study ocean related phenomena, such as surface waves, sea ice, internal waves, currents and wind. The great advantage of SAR over for instance optical imagery is that it operates at wavelengths that are generally unaffected by the cloud cover. Also, it does not require solar illumination, meaning it can operate day and night. Another advantage is that factors such as the frequency, incident angle, polarization, swath width and spatial resolution can be controlled. SAR is an active microwave remote sensing technique. A microwave is sent to an object and the radar measures the intensity backscatter and phase. Standard frequencies of the SAR sensors are X-, C-, S-, L- and P-bands, equivalent to a wavelength of 3 – 75 cm. SAR determines its along-track (azimuth) position by the instantaneous Doppler shift of the reflected signal (e.g., Massonnet & Souyris 2008). This is where SAR differs from real aperture radar (RAR). The major limitation of RAR is that its azimuth resolution is directly proportional to the physical length of the antenna.

5.1. Imaging of ocean waves in open water

Ocean surface imaging by SAR is undoubtedly the least understood and most complex data produced by remote sensing (Holt, 2004). This is because the imaging process is sensitive to a numerous number of parameters, including the motion of the ocean waves, the geometry and properties of the SAR instrument itself.

A SAR image over the ocean consists of a backscatter map and the reflectivity of the radar return is called the Normalized Radar Cross Section (NRCS). The main processes that are responsible for the backscatter depend on the incidence angle. For small incidence angles (< 20°), specular reflection dominates. This reflection is identical to an ordinary mirror, where the angle of the reflected signal is the same as the angle of incidence (Thompson, 2004). However, SAR satellites such as the Sentinel-1 typically operates at incidence angles between 25 and 45°, where Bragg scattering dominates (Valenzuela, 1978). Under Bragg scattering, also referred to as resonance scattering, the radar signal is scattered back by short, wind generated wave components whose wavelength is close to the radar frequency (Holt, 2004).

As mentioned, Bragg scattering mainly reflects the emitted signal. This backscatter is however modulated by three processes which are: hydrodynamic modulation, tilt modulation, and velocity bunching (see for instance: Alpers & Rufenach, 1979; Alpers et al., 1981; Alpers, 1983; Hasselmann et al., 1985). The hydrodynamic modulation is a result of the orbital velocities of long waves. These velocities have different directions along the wave, creating zones of convergence (crest) and divergence (trough). Therefore, on the crest of long waves, the short waves are compressed, and Bragg scattering is increased. The long waves do not only modify the dynamics of the short waves, but also change the local orientation (tilt). This is referred to as tilt modulation. Velocity bunching is caused by the motion of the ocean waves relative to the motion of the satellite. The sea surface motion introduces an extra Doppler shift, which is used to determine its azimuth position and hence, the scatterer or echoes will be misplaced. The periodic motion of the long waves causes an apparent increase and decrease in scatter density, allowing long waves to be visible in SAR imagery. The velocity bunching of short waves also cause random position shifts in azimuth direction and results in an apparent blurring of the SAR image (e.g., Raney 1981). The degraded azimuth resolution results in the well-known azimuth cut-off (Kerbaol et al., 1998). SAR does not sense waves that are shorter than the azimuth cut-off wavelength. It is important to note that velocity bunching modulation is largest for waves traveling in azimuth and disappears for waves traveling in range direction. An example of ocean wave imaging by Sentinel-1 SAR is given in Figure 4. Wave diffraction around Bear Island can be seen. The waves enter the image at the bottom right corner and travel towards the top left corner, i.e., the propagation direction is in between range and azimuth. At the top left of the figure, the waves have diffracted around the island and now travel in range direction. These waves appear much clearer in the image than the waves in the bottom right corner, which is due to

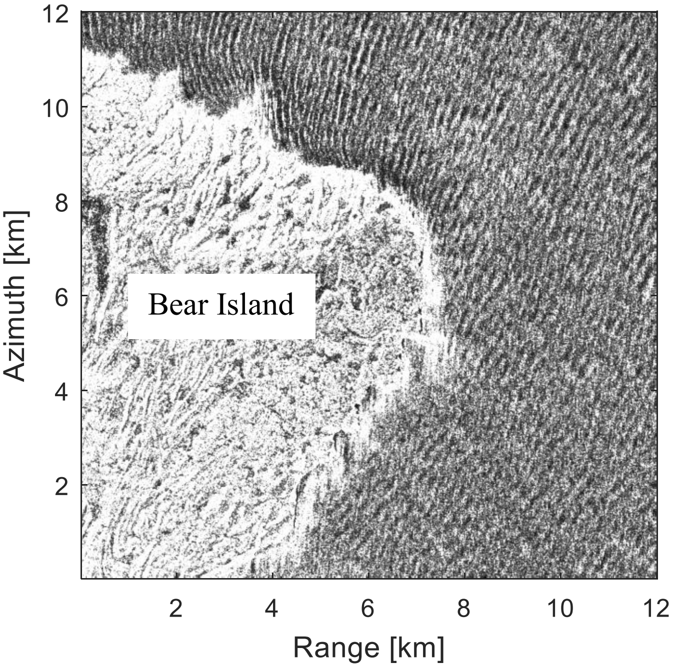

Figure 4. SAR imagery of ocean waves diffracting around Bear Island, located in the Barents Sea. The normalized intensity from a Sentinel-1 GRD product is shown, acquired on the 15th of January 2018 at 05:35:26 UTC.

the difference in the velocity bunching modulation for waves traveling in range and azimuth direction.

It is possible to compute the 2D wave spectrum from SAR imagery for waves that are larger than the cut-off wavelength. Following spectral analysis, the intensity variance spectrum can directly be obtained from SAR images. However, to obtain the real wave spectrum one would have to correct for the three modulation mechanisms and the function that does this is called the modulation transfer function (e.g., Vachon et al., 2004). For a more detailed introduction to ocean wave imaging by SAR see for instance (Bruck, 2015; Husson, 2012; Jackson and Apel, 2004).

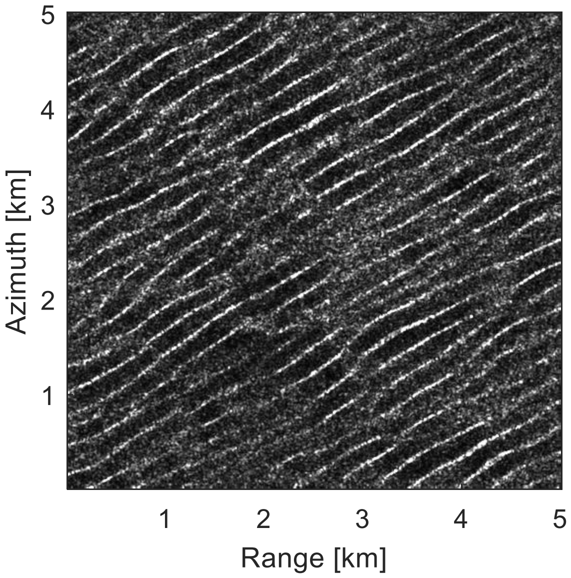

Figure 5. Typical image of long waves within the sea ice. The image is acquired on the 4th of April 2017 at 15:03:19 UTC, just East of Svalbard.

5.2. Imaging of ocean waves in sea ice

SAR has shown to be able to detect ocean wind waves and swell waves within the sea ice cover. The first observations were made by airborne SAR in the late 1980's and beginning 1990's (Lyzenga et al., 1985; Carsey et al., 1989; Raney et al., 1989; Liu et al., 1991a). The first SAR images obtained from satellites came from Seasat (Fu and Holt, 1982) and one of the most recent launched SAR satellites is the Sentinel-1 constellation.

Ocean waves create patterns in SAR images over the sea ice such as shown in Figure 5. When these patterns are visible in the imagery, the peak wavelength and dominant wave direction can be determined from the image intensity spectrum (Liu et al., 1991a; Schulz-Stellenfleth & Lehner 2002). Multiple studies investigated the change in peak wavelength and dominant wave direction as ocean waves propagate into the MIZ (Gebhardt et al., 2016; A. K. Liu et al., 1991; Monteban et al., 2019; Shen et al., 2018). The peak wavelength increases because the ice cover acts as a low pass filter, damping out the high frequency waves. The dominant wave direction changes due to refraction at the ice edge. However, part of the change in dominant wave direction at the ice edge is an imaging artifact of SAR (Monteban et al., 2019; Schulz-Stellenfleth and Lehner, 2002).

The study of Lyzenga et al. (1985) used SAR imagery of sea ice to show that velocity bunching is the dominant mechanism for waves to be visible within the sea ice. They showed that due to velocity bunching, straight lines such as the ice edge appear as oscillating lines in the images. Ardhuin et al. (2015) used the periodical displacement that results in bright oscillating lines in the ice pack to estimate the orbital velocities, which can be related to the significant wave height when two swell systems are present. Ardhuin et al. (2017) extended this to a methodology to derive the wave spectra, by relating wave patterns visible in the SAR imagery (e.g., Figure 5) to orbital velocities. This method was applied by Stopa et al. (2018a), together with a homogeneity test, based on the homogeneity parameter of (Koch, 2004). A storm event in the Beaufort Sea was captured by Sentinel-1 IW and the wave evaluation over a length of 400 km into the MIZ was studied. They found that wave heights have an attenuation coefficient that varies spatially, which suggest that ice modules in numerical wave models should have multiple wave decay mechanisms. Furthermore, these measurements from SAR were used by Ardhuin et al. (2018) to validate the operational numerical wave model WAVEWATCH III and to test multiple processes that affect ocean waves within the sea ice. The largest dataset of wave attenuation up to date is given by Stopa et al. (2018b) obtained at the Southern Ocean using the

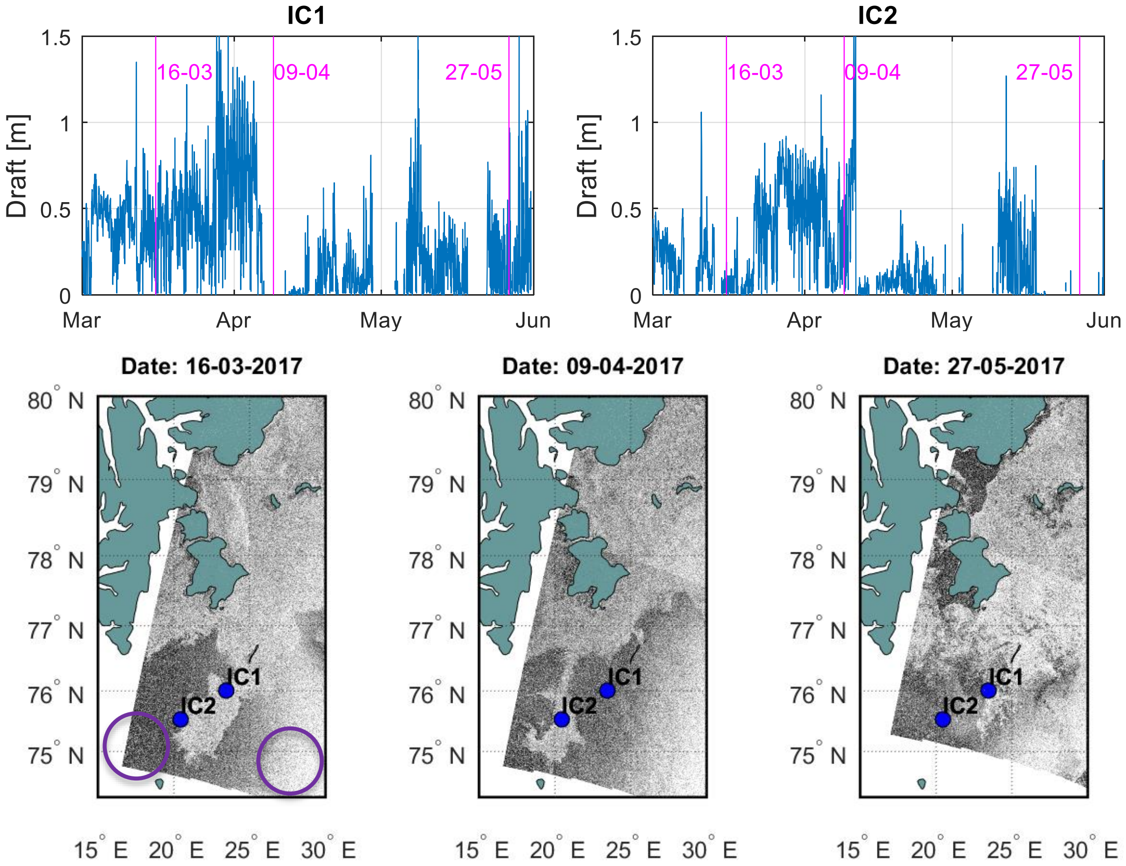

Figure 6. Comparison of the ice draft data at the ice mooring stations IC1 and IC2 with Sentinel-1 EW imagery for three different dates in the year 2017. The Sentinel-1 EW images show the normalized intensity in gray scale.

method of Ardhuin et al., (2015, 2017) and Stopa et al., (2018a). There is in general a weaker attenuation for long waves and a very large scatter (up to 3 orders of magnitude) is observed.

Sea ice affects the ocean waves by, amongst others, changes in the dispersion relation (e.g., Collins et al., 2017). Many different formulations of the wave dispersion relation exist in the literature, but all are a function of the ice thickness. With SAR observations, it is possible to estimate the ice thickness by inverting the wave dispersion relation. This was first done using the mass loading model (Wadhams et al., 2002; Wadhams and Holt, 1991). However, a severe overestimation was found. Later, the viscous layer model was used and good estimates of the ice thickness were obtained (Wadhams et al., 2018, 2004).

5.3. Ice edge

The sea ice terrain is most complex since there are many possible forms of ice and because sea ice properties and the structure are constantly altered by ocean and atmospheric processes. The amount of backscatter from sea ice depends, amongst others, on the surface parameters and is naturally different from the open ocean. The difference in intensity backscatter between the open water and the sea ice can be used to determine the position of the ice edge. Multiple algorithms have been written that automatically find the location of the ice edge (e.g., Liu et al., 1997; Liu et al., 2016; Similä et al., 2013). In Figure 6, we qualitatively show the position of the ice edge around the BaSMIN study site using Sentinel-1 Extra Wide (EW) swath images, acquired on three different dates. The sea ice appears brighter than the open ocean and the ice edge can straightforward be observed. For instance, on the 9th of April 2017, we can see that ice mooring IC2 is circumpassed by the sea ice while ice mooring IC1 is not. This agrees with the ice draft data at these mooring stations as shown in the upper panel of Figure 6. Further, when looking at the Sentinel-1 EW image on the 16th of April 2017, we can see that the brightness on the open water is larger at the east side than on the west side (compare the

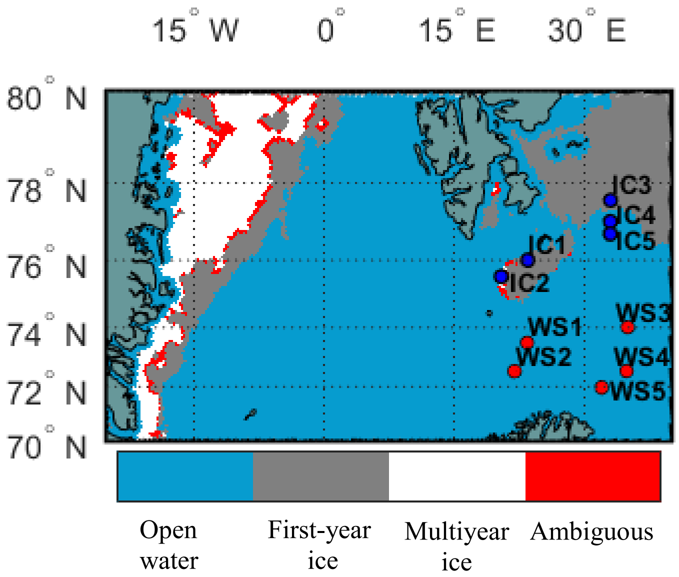

Figure 7. Ice type map for the 1st of March 2018. The data are taken from the dataset Sea ice type product of the EUMETSAT Ocean and Sea Ice Satellite Application Facility (OSI SAR, www.osi-saf.org).

brightness in the purple circles in Figure 6). This is because the incidence angle on the east side is much smaller and some specular reflection occurs here.

5.4. Floe size distribution

To understand the complex dynamics of the Arctic MIZ it is essential to have floe size distribution data. However, floe size distribution data from satellites are quite rare due to the lack of reliable algorithms (Hwang et al., 2017). Some of the challenges encountered include: variability in intensity backscatter, high level of noise, presence of melt ponds, and lack of a method to properly distinguish between adjacent floes in contact. Recently, an algorithm was developed by Hwang et al. (2017) to semi-automatically retrieve floe size distributions from SAR data. Their algorithm performs well for floe sizes larger than 100 m in diameter. Floe sizes smaller than 100 m diameter are usually not detected by the algorithm. With the increasing coverage and spatial resolution of SAR satellites nowadays, it is only to be expected that these algorithms will improve in the future. It will be very interesting to understand the coupling between certain wave events and the floe size distribution. This will be possible in the future when the algorithms improve, and a large dataset becomes available.

5.5. Ice type

The backscatter from sea ice varies, as the characteristics of the illuminated area are different, i.e., different ice forms and properties. Backscatter response is different during winter and summer times and there are four surface parameters that affect the scattering characteristics: the surface roughness, the dielectric constant, dielectric discontinuities (e.g., gas bubbles) and the orientation of the sea ice (Onstott and Shuchman, 2004). Therefore, the intensity backscatter consists of surface and volume scattering. Furthermore, the appearance of sea ice in SAR images is also affected by: the frequency of the SAR sensor, the polarization, the incidence angle, the noise level and the spatial resolution (Dierking, 2013). Considerable efforts have been dedicated over the last few decades to understand the sensitivity of the radar backscatter for various ice properties and different SAR sensor configurations (frequency, polarization, etc.). For instance, surface scattering dominates the backscatter from first-year ice and can be very low if the ice is formed under calm conditions and is therefore very smooth (specular reflection). Multi-year ice is less saline and has a greater microwave penetration depth, i.e., volume scattering dominates. This leads to a higher backscatter return than for first-year ice (Onstott and Shuchman, 2004).

Combining data from different satellite sensors made it possible to produce maps giving the type of ice. An example of an ice type map that includes the study site of the BaSMIN programme is given in Figure 7. It has a resolution of 10 km and is among other things based on the sensors: ASCAT, AMSR-2 and SSMIS. From the figure, it can be seen that on this date there is only first-year ice around the study site. Multi-year ice can be observed at the east side of Greenland.

6. Conclusions

In this study we reviewed three different types of satellite remote sensing, including optical, altimetry and SAR. To illuminate the review, we used remote sensing data acquired by ESA's Sentinel missions over the BaSMIN study site. We show how in situ data can be used in combination with remote sensing observations to provide a clearer picture. Moreover, the in-situ data can be used to validate multiple remote sensing observations, and hence increase the confidence we have in them.

Optical imagery can provide high resolution and high-quality images, up to 10-meter resolution for Sentinel-2. However, optical sensors require solar illumination and cloud free conditions. This severely limits the number of usable images, especially in the Polar regions.

Altimetry data provides, amongst others, very accurate significant wave height data in the open ocean. In this study we used Sentinel-3 wave height data and compared it with the buoy measurements obtained during the BaSMIN programme. We used satellite tracks that are within a radius of 20 km of the wave buoys, which resulted in 276 observations for the year 2018. The comparison shows very good results with an RMSE of 0.46 and an R^2 value of 0.86. In addition, altimetry can provide information regarding the sea ice freeboard, which can be used to calculate the ice thickness.

SAR data are the most useful source of information in the Polar regions as it provides information over large spatial scales and does not require solar illumination or cloud free conditions. SAR has been used to study wave propagation within the sea ice and an increase in peak wavelength, change in dominant wave direction and wave attenuation have been reported in literature. Furthermore, SAR can be used to determine the position of the ice edge and distinguish between ice type (e.g., first and multi-year ice). Floe size distributions can be estimated, but the algorithms so far are not very reliable and only work for large floe sizes.

Overall, satellite remote sensing observations are a very valuable source in order to study wave-ice interactions. Data over large spatial areas can be obtained for a relatively low cost. It should however be combined with in situ data as much as possible. In this way, information in the temporal domain and spatial domain are combined, which provide the clearest picture of the processes at play.

Acknowledgements

We would like to thank and acknowledge Equinor (former Statoil) and the other BaSMIN JIP members for kindly making the data recorded in the Barents Sea available for this project. The Sentinel-1, Sentinel-2 and Sentinel-3 data are provided by the European Space Agency (ESA) and can freely be downloaded from ESA's Sentinel data hub. Further we would like to acknowledge the support from the SAMCoT CRI through the Research Council of Norway and all the SAMCoT partners.

References

ACIA, 2004. Impacts of a Warming Arctic: Arctic Climate Impact Assessment. ACIA Overv. Rep. 140. https://doi.org/10.2277/0521617782

Alpers, W., 1983. Monte Carlo Simulations for Studying the Relationship Between Ocean Wave and Synthetic Aperture Radar Image Spectra. J. Geophys. Res. 88, 1745–1759.

Alpers, W., Rufenach, C., 1979. The effect of orbital motions on synthetic aperture radar imagery of ocean waves. IEEE Trans. Antennas Propag. 27, 685–690. https://doi.org/10.1109/TAP.1979.1142163

Alpers, W.R., Ross, D.B., Rufenach, C.L., 1981. On the detectability of ocean surface waves by real and synthetic aperture radar. J. Geophys. Res. Ocean. 86, 6481–6498. https://doi.org/10.1029/JC086iC07p06481

Ardhuin, F., Boutin, G., Stopa, J., Girard-Ardhuin, F., Melsheimer, C., Thomson, J., Kohout, A., Doble, M., Wadhams, P., 2018. Wave Attenuation Through an Arctic Marginal Ice Zone on 12 October 2015. 2. Numerical Modeling of Waves and Associated Ice Breakup. J. Geophys. Res. Ocean. 1–17. https://doi.org/10.1029/2018JC013791

Ardhuin, F., Collard, F., Chapron, B., Girard-Ardhuin, F., Guitton, G., Mouche, A., Stopa, J.E., 2015. Estimates of ocean wave heights and attenuation in sea ice using the SAR wave mode on Sentinel-1A. Geophys. Res. Lett. 42, 2317–2325. https://doi.org/10.1002/2014GL062940

Ardhuin, F., Stopa, J., Chapron, B., Collard, F., Smith, M., Thomson, J., Doble, M., Blomquist, B., Persson, O., Collins, C.O., Wadhams, P., 2017. Measuring ocean waves in sea ice using SAR imagery: A quasi-deterministic approach evaluated with Sentinel-1 and in situ data. Remote Sens. Environ. 189, 211–222. https://doi.org/10.1016/j.rse.2016.11.024

Born, G.H., Dunne, J.A., Lame, D.B., 1979. Seasat Mission Overview. Am. Assoc. Adv. Sci. 204, 1405–1406.

Broström, G., Christensen, K., 2008. Waves in sea ice. Met.No Rep.

Bruck, M., 2015. Sea State measurements usiong TerraSAR-X/TanDEM-X data (PhD Thesis). Kiel.

Carsey, F.D., Argus, S.A.D., Collins, M.J., Holt, B., Livingstone, C.E., Tang, C.L., 1989. Overview of LIMEX'87 ice observations. IEEE Trans. Geosci. Remote Sens. 27, 468–482. https://doi.org/10.1109/TGRS.1989.35930

Collins, C.O., Rogers, W.E., Lund, B., 2017. An investigation into the dispersion of ocean surface waves in sea ice. Ocean Dyn. 67, 263–280. https://doi.org/10.1007/s10236-016-1021-4

Dierking, W., 2013. Sea Ice Monitoring by Synthetic Aperture Radar. Oceanography 26, 100–111. https://doi.org/10.5670/oceanog.2013.33

Drusch, M., Del Bello, U., Carlier, S., Colin, O., Fernandez, V., Gascon, F., Hoersch, B., Isola, C., Laberinti, P., Martimort, P., Meygret, A., Spoto, F., Sy, O., Marchese, F., Bargellini, P., 2012. Sentinel-2: ESA's Optical High-Resolution Mission for GMES Operational Services. Remote Sens. Environ. 120, 25–36. https://doi.org/10.1016/j.rse.2011.11.026

European Space Agency, 2013. Sentinel-3 User Handbook. https://doi.org/GMES-S1OP-EOPG-TN-13-0001

European Space Agency, 2012. Sentinel-3: ESA's Global Land and Ocean Mission for GMES Operational Services. Esa Sp-1322/3 97.

Fu, L., Holt, B., 1982. Seasat views oceans with synthetic-aperture radar. JPL Publ. 81-120 204. https://doi.org/10.1111/j.1365-2133.2012.11180.x

Gebhardt, C., Bidlot, J.R., Gemmrich, J., Lehner, S., Pleskachevsky, A., Rosenthal, W., 2016. Wave observation in the marginal ice zone with the TerraSAR-X satellite. Ocean Dyn. 66, 839–852. https://doi.org/10.1007/s10236-016-0957-8

Guerreiro, K., Fleury, S., Zakharova, E., Kouraev, A., Rémy, F., Maisongrande, P., 2017. Comparison of CryoSat-2 and ENVISAT radar freeboard over Arctic sea ice: Toward an improved Envisat freeboard retrieval. Cryosphere 11, 2059–2073. https://doi.org/10.5194/tc-11-2059-2017

Hasselmann, K., Raney, R.K., Plant, W.J., Alpers, W., Shuchman, R.A., Lyzenga, D.R., Rufenach, C.L., Tucker, M.J., 1985. Theory of synthetic aperture radar ocean imaging: A MARSEN view. J. Geophys. Res. 90, 4659. https://doi.org/10.1029/JC090iC03p04659

Holt, B., 2004. Chapter 2. SAR Imaging of the Ocean Surface, in: Synthetic Aperture Radar Marine User's Manual. pp. 25–79.

Husson, R., 2012. Development and validation of a global observation-based swell model using wave mode operating Synthetic Aperture Radar. Université de Bretagne, Brest.

Hwang, B., Ren, J., McCormack, S., Berry, C., Ben Ayed, I., Graber, H.C., Aptoula, E., 2017. A practical algorithm for the retrieval of floe size distribution of Arctic sea ice from high-resolution satellite Synthetic Aperture Radar imagery. Elem Sci Anth 5, 38. https://doi.org/10.1525/elementa.154

Jackson, C.R., Apel, J.R., 2004. Synthetic Aperture Radar: Marine User's Manual. https://doi.org/10.1016/S0165-4101(01)00024-6

Jakobsson, M., Mayer, L., Coakley, B., Dowdeswell, J.A., Forbes, S., Fridman, B., Hodnesdal, H., Noormets, R., Pedersen, R., Rebesco, M., Schenke, H.W., Zarayskaya, Y., Accettella, D., Armstrong, A., Anderson, R.M., Bienhoff, P., Camerlenghi, A., Church, I., Edwards, M., Gardner, J. V., Hall, J.K., Hell, B., Hestvik, O., Kristoffersen, Y., Marcussen, C., Mohammad, R., Mosher, D., Nghiem, S. V., Pedrosa, M.T., Travaglini, P.G., Weatherall, P., 2012. The International Bathymetric Chart of the Arctic Ocean (IBCAO) Version 3.0. Geophys. Res. Lett. 39, 1–6. https://doi.org/10.1029/2012GL052219

Kerbaol, V., Chapron, B., Vachon, P.W., 1998. Analysis of ERS-1/2 synthetic aperture radar wave mode imagettes. J. Geophys. Res. Ocean. 103, 7833–7846. https://doi.org/10.1029/97JC01579

Koch, W., 2004. Directional analysis of SAR images aiming at wind direction. IEEE Trans. Geosci. Remote Sens. 42, 702–710. https://doi.org/10.1109/TGRS.2003.818811

Kohout, A.L., Williams, M.J.M., Toyota, T., Lieser, J., Hutchings, J., 2016. In situ observations of wave-induced sea ice breakup. Deep. Res. Part II Top. Stud. Oceanogr. 131, 22–27. https://doi.org/10.1016/j.dsr2.2015.06.010

Komen, G., Cavaleri, L., Donelan, M., Hasselmann, K., Hasselmann, S., Janssen, P., 1994. Dynamics and Modelling of Ocean Waves. Cambridge University Press, Cambridge.

Kudryavtsev, V., Yurovskaya, M., Chapron, B., Collard, F., 2017. Sun glitter imagery of surface waves. Part 2:Waves transformation on ocean currents. J. Geophys. Res. 1384–1399. https://doi.org/10.1002/2016JC012425.Sun

Liu, A.K., Holt, B., Vachon, P.W., 1991a. Wave propagation in the marginal ice zone: Model predictions and comparisons with buoy and synthetic aperture radar data. J. Geophys. Res. Ocean. 96, 4605–4621. https://doi.org/10.1029/90JC02267

Liu, A.K., Martin, S., Kwok, R., 1997. Tracking of ice edges and ice floes by wavelet analysis of SAR images. J. Atmos. Ocean. Technol. 14, 1187–1198. https://doi.org/10.1175/1520-0426(1997)014<1187:TOIEAI>2.0.CO;2

Liu, A.K., Vachon, P.W., Peng, C.Y., 1991b. Observation of wave refraction at an ice edge by Synthetic Aperture Radar. J. Geophys. Res. 96, 4803–4808. https://doi.org/10.1029/90JC02546

Liu, J., Scott, K.A., Gawish, A., Fieguth, P., 2016. Automatic detection of the ice edge in SAR imagery using curvelet transform and active contour. Remote Sens. 8, 1–16. https://doi.org/10.3390/rs8060480

Lyzenga, D.R., Shuchman, R. a., Lyden, J.D., 1985. SAR Imaging of Waves in Water and Ice : Evidence for Velocity Bunching. J. Geophys. Res. 90, 1031–1036. https://doi.org/10.1029/JC090iC01p01031

Massonnet, D., Souyris, J.-C., 2008. Imaging with Synthetic Aperture Radar.

Monteban, D., Lubbad, R., Johnsen, H., 2019. Sentinel-1 SAR observations of peak wavelength and wave direction in the marginal ice zone of the Barents Sea, in: POAC Port and Ocean Engineering under Arctic Conditions.

Müller, F.L., Dettmering, D., Bosch, W., Seitz, F., 2017. Monitoring the arctic seas: How satellite altimetry can be used to detect openwater in sea-ice regions. Remote Sens. 9. https://doi.org/10.3390/rs9060551

Onstott, R.G., Shuchman, R. a., 2004. Chapter 3. SAR Measurements of Sea Ice, in: SAR Marine User's Manual. pp. 81–115.

Raney, R.K., 1981. Wave Orbital Velocity Fade & Sar Response To Azimuth Waves. IEEE J. Ocean. Eng. OE-6, 140–146. https://doi.org/10.1109/JOE.1981.1145495

Raney, R.K., Vachon, P.W., Abreu, R.A., Bhogal, A.S., 1989. Airborne SAR Observations of

Ocean Surface Waves Penetrating Floating Ice. IEEE Trans. Geosci. Remote Sens. 27, 492–500.

Schulz-Stellenfleth, J., Lehner, S., 2002. Spaceborne synthetic aperture radar observations of ocean waves traveling into sea ice. Geophys. Res. Lett. 107, 1–19.

Shen, H., Perrie, W., Hu, Y., He, Y., 2018. Remote Sensing of Waves Propagating in the Marginal Ice Zone by SAR. J. Geophys. Res. Ocean. 123, 189–200. https://doi.org/10.1002/2017JC013148

Similä, M., Dinessen, F., Hughes, N.E., Mäkynen, M., 2013. Ice Edge Detection With Dual-polarized Sar Data. POAC'13 Proc.

Solomon, S.M., 2005. Spatial and temporal variability of shoreline change in the Beaufort-Mackenzie region, northwest territories, Canada. Geo-Marine Lett. 25, 127–137. https://doi.org/10.1007/s00367-004-0194-x

Squire, V.A., 2007. Of ocean waves and sea-ice revisited. Cold Reg. Sci. Technol. 49, 110–133. https://doi.org/10.1016/j.coldregions.2007.04.007

Squire, V.A., Duggan, J.P., Wadhams, P., Rottier, P.J., Liu, A.J., 1995. Of ocean waves and sea ice. Annu. Rev. Fluid Mech. 27, 115–168. https://doi.org/10.1146/annurev.fl.27.010195.000555

Stopa, J.E., Ardhuin, F., Thomson, J., Smith, M.M., Kohout, A., Doble, M., Wadhams, P., 2018a. Wave Attenuation Through an Arctic Marginal Ice Zone on 12 October 2015. 1. Measurement of Wave Spectra and Ice Features From Sentinel 1A. J. Geophys. Res. Ocean. 123, 3619–3634. https://doi.org/10.1029/2018JC013791

Stopa, J.E., Sutherland, P., Ardhuin, F., 2018b. Strong and highly variable push of ocean waves on Southern Ocean sea ice. Proc. Natl. Acad. Sci. U. S. A. 237, 1–5. https://doi.org/10.1073/pnas.1802011115

Thompson, D.R., 2004. Chapter 4. Microwave Scattering from the Sea, in: Synthetic Aperture Radar Marine User's Manual. pp. 117–138.

Tilling, R.L., Ridout, A., Shepherd, A., 2018. Estimating Arctic sea ice thickness and volume using CryoSat-2 radar altimeter data. Adv. Sp. Res. 62, 1203–1225. https://doi.org/10.1016/j.asr.2017.10.051

Vachon, P.W., Monaldo, F.M., Holt, B., Lehner, S., 2004. Chapter 5. Ocean Surface Waves and Spectra, in: SAR Marine User's Manual. pp. 139–169.

Valenzuela, G.R., 1978. Theories for the interaction of electromagnetic and oceanic waves - A review. Boundary-Layer Meteorol. 13, 61–85. https://doi.org/10.1007/BF00913863

Vu, P.L., Frappart, F., Darrozes, J., Ramillien, G., Marieu, V., Blarel, F., Bonnefond, P., 2018. Jason-3 and Sentinel-3A Altimeter Validation Along the French Atlantic Coast in the Southern Bay of Biscay. IGARSS 2018 - 2018 IEEE Int. Geosci. Remote Sens. Symp. 3793–3796. https://doi.org/10.1109/IGARSS.2018.8519532

Wadhams, P., Aulicino, G., Parmiggiani, F., Persson, P.O.G., Holt, B., 2018. Pancake Ice Thickness Mapping in the Beaufort Sea From Wave Dispersion Observed in SAR Imagery. J. Geophys. Res. Ocean. 123, 2213–2237. https://doi.org/10.1002/2017JC013003

Wadhams, P., Holt, B., 1991. Waves in frazil and pancake ice and their detection in Seasat synthetic aperture radar imagery. J. Geophys. Res. 96, 8835–8852. https://doi.org/10.1029/91JC00457

Wadhams, P., Parmiggiani, F., de Carolis, G., 2002. The Use of SAR to Measure Ocean Wave Dispersion in Frazil–Pancake Icefields. J. Phys. Oceanogr. 32, 1721–1746. https://doi.org/10.1175/1520-0485(2002)032<1721:TUOSTM>2.0.CO;2

Wadhams, P., Parmiggiani, F.F., De Carolis, G., Desiderio, D., Doble, M.J., 2004. SAR imaging of wave dispersion in Antarctic pancake ice and its use in measuring ice thickness. Geophys. Res. Lett. 31, L15305. https://doi.org/10.1029/2004GL020340